JOURNAL OF Materials CHEMISTRY

Spectroscopic properties of microporous layered tin sulfide materials

Tong Jiang, Geoffrey A. Ozin*[a] and Robert L. Bedard[b]

[a] *Materials Chemistry Research Group, Department of Chemistry, University of Toronto, Toronto, Ontario, Canada, M5S 3H6*

[b] *Universal Oil Product, 25 E. Algonquin Rd., Des Plaines, Illinois, 60017, USA*

^{119}Sn solid state nuclear magnetic resonance, ^{119}Sn Mössbauer, Fourier transform Raman and variable temperature single crystal UV–VIS absorption, emission and excitation spectra of some archetypal microporous layered tin sulfides, denoted $(Et_4N)_2Sn_3S_7$ (TEA-SnS-1), $(C_6H_{12}N_2H)_2Sn_3S_7$ (DABCOH-SnS-1), $(NH_4)_{0.5}(Et_4N)_{1.5}Sn_3S_7$ (ATEA-SnS-1) and $(Pr_4N)_2Sn_4S_9$ (TPA-SnS-3), are reported. The combined spectroscopic results provide a rather comprehensive picture of structure–property relations for this novel class of solids, which have the unusual ability of being able to behave as both molecular sieve and intercalation materials to a range of guests.

Introduction

The synthesis and single crystal X-ray diffraction structures of crystals grown under earth-based gravity and space-based microgravity conditions,[1,2] surface topology and microstructure,[3] intermediates and mode of formation,[4] framework flexibility,[5] thermochemical,[6] adsorption and sensing properties,[7] of various members of the new class of microporous layered tin sulfide materials, denoted SnS-*n*, have recently been reported. These materials are rather unusual as they can display both molecular sieving and intercalation behaviour to a range of guests.[8] In this paper we focus attention on some spectroscopic properties of these materials. Specifically, solid-state ^{119}Sn NMR, ^{119}Sn Mössbauer and FT-Raman spectroscopies are employed to provide local details about coordination geometry and electron distribution around the tin centers, while single crystal UV–VIS absorption, luminescence and excitation spectroscopy are used to probe electronic detail on larger length scales. Whether quantum size effects contribute to the electronic properties of SnS-*n* materials is an interesting question.[9] Attention will mainly be directed to the group of structurally well defined microporous layered tin sulfides, denoted $(Et_4N)_2Sn_3S_7$ (TEA-SnS-1), $(C_6H_{12}N_2H)_2Sn_3S_7$ (DABCOH-SnS-1), $(NH_4)_{0.5}(Et_4N)_{1.5}Sn_3S_7$ (ATEA-SnS-1) and $(Pr_4N)_2Sn_4S_9$ (TPA-SnS-3).

^{119}Sn CP-MAS NMR Spectroscopy

DABCOH-SnS-1

A series of CP-MAS ^{119}Sn NMR measurements were conducted with variable contact time in the range 1–16 ms and a recycle time of 10 s. The greatest enhancement was achieved with a contact time of 2 ms. Fig. 1 displays the experimental (contact time, CT = 2 ms) and calculated spectra based on the Herzfeld and Berger method.[10] Fifteen peaks are observed that are equally spaced by 5 kHz, the MAS spinning rate. Therefore, there is only one isotropic CS resonance frequency, the rest are spinning side bands. The signal which occurred at −343.8 ppm always remains at this position regardless of the spinning rate, and therefore is identified as the isotropic chemical shift line. The calculated chemical shift (CS) tensors are at −52, −43 and 18 kHz, Table 1.

There are 3 crystallographically distinct tin sites in DABCOH-SnS-1, namely the 3 pseudo-trigonal bipyramidal (PTBP) tin centers constituting a Sn_3S_4 broken-cube cluster.[1] As shown in Fig. 2, each pseudo-trigonal bipyramidal SnS_5 has three equatorial Sn—S bonds ranging from 2.370 to 2.411 Å, and two long axial Sn—S bonds ranging from 2.496 to 2.609 Å. The equatorial sulfurs slightly bend towards the three coordinated capping-sulfur residing at the middle of the broken-cube cluster. The angles between the two axial S—Sn—S bonds range from 175.0 to 179.5 Å among the three tin sites. Clearly, the local Sn—S geometry and bonding among the three tin sites is quite similar, and consequently they are expected to have similar chemical shift anisotropy (CSA) patterns. The failure to resolve them by ^{119}Sn CP-MAS NMR spectroscopy is consistent with the single crystal structure data.[1] The orthorhombic CSA lineshape agrees with the

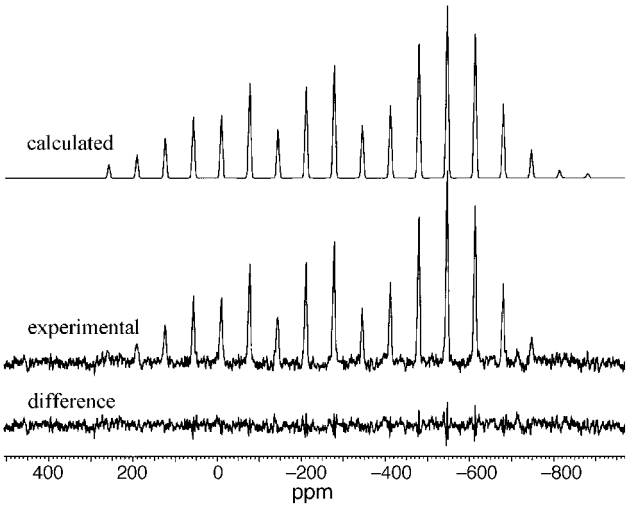

Fig. 1 Solid state ^{119}Sn CP-MAS NMR spectra of DABCOH-SnS-1, collected at a contact time of 2 ms and spinning rate of 5 kHz.

Table 1 Summary of ^{119}Sn NMR data for SnS-1 and SnS-3 materials

	C.N.[a]	δ_{iso}[b]	σ_{11}[c]/kHz	σ_{22}[c]/kHz	σ_{33}[c]/kHz
$(CHA)_4Sn_2S_6$	4	67.3	23	23	−31
DABCOH-SnS-1	5	−343.8	−52	−43	18
ATEA-SnS-1	5	−352.1	−57	−45	22
TPA-SnS-3	4	−4.9	−6	−4	9
	4	−20.2	−8	−8	11
	5	−306.0	−48	−48	27
	5	−343.2	−54	−45	22
	5	−320.6	31	9	−111
	5	−326.4	23	11	−107

[a] C.N. = coordination number. [b] ±0.3 ppm. [c] ±1 kHz.

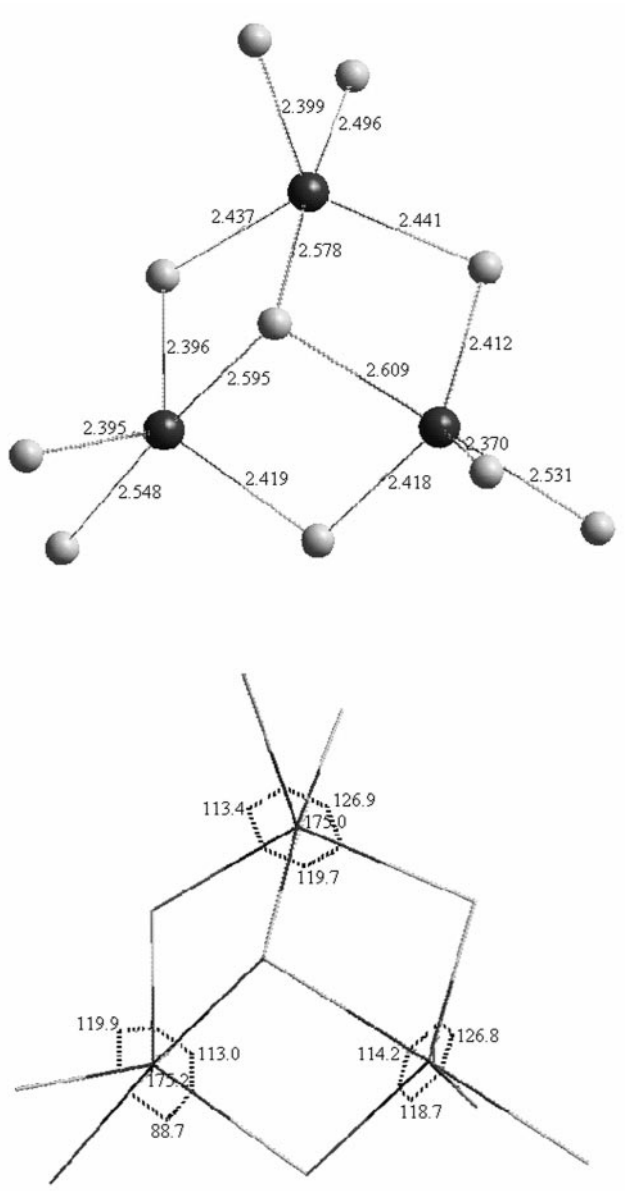

Fig. 2 An illustration of the local bonding geometry around the tin centers in DABCOH-SnS-1, important bond lengths and angles are displayed

pseudo-trigonal bipyramidal coordination environment around the tin centers. However, the relatively small value of the asymmetry parameter η (0.2) suggests that the electric field gradient and local electron distribution around the tin center are rather symmetric. It is interesting to note the nearly 70 kHz or 950 ppm spread of the CSA for the pseudo-trigonal bipyramidal tin sites in DABCOH-SnS-1. The isotropic CS value for the distorted pseudo-trigonal bipyramidal tin sites in $Na_4Sn_3S_8$ has been recently reported at -359.6 ppm with a CSA spread width of 931 ppm.[11]

ATEA-SnS-1

The ^{119}Sn CP-MAS spectrum of ATEA-SnS-1 collected at a spinning rate of 8 kHz displays a similar CSA lineshape to that of DABCOH-SnS-1. One isotropic band is found at -352.1 ppm with the principle CSA tensors of -57, -45 and 22 kHz. As discussed above for DABCOH-SnS-1, ATEA-SnS-1 also has three crystallographically distinct, pseudo-trigonal bipyramidal tin sites that possess a quite similar local Sn—S geometry and bonding character. Consequently they display

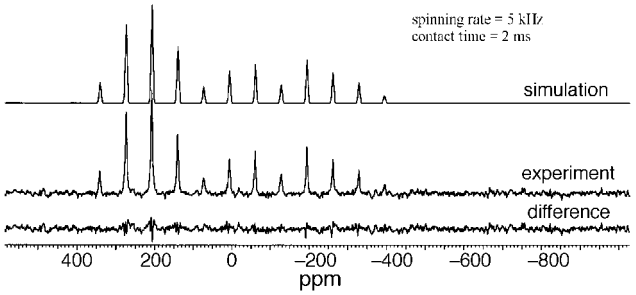

Fig. 3 ^{119}Sn CP-MAS spectrum of the reference cyclohexylammonium tin sulfide dimer $(CHA)_4Sn_2S_6$

similar CSA lineshapes which are not resolved by solid state ^{119}Sn MAS NMR spectroscopy.

$(CHA)_4Sn_2S_6$

The CP-MAS ^{119}Sn NMR spectrum of the reference cyclohexylammonium (CHA) dimeric tin sulfide material, $(CHA)_4Sn_2S_6$,[4] is displayed in Fig. 3 with a spinning rate of 5 kHz. Only one CSA pattern is resolved after deconvolution based on the Herzfeld and Berger method.[10] This is consistent with its single crystal structure[4] in which one crystallographically distinct and distorted T_d tin site is present. The isotropic CS value is found at 67.2 ppm. The presence of a relatively large CSA width of 54 kHz is consistent with its distorted T_d geometry. The CS value of the nearly perfect T_d tin site in Na_4SnS_4 is reported to be 67.6 ppm with a very small CSA spread of less than 7.5 kHz when spinning at 4.5 kHz.[11] In comparison, the chemical shift value for the octahedral tin in berndtite SnS_2 appears at -765 ppm[11] while the pseudo-trigonal bipyramidal tin in the SnS-1 materials occurs at about -340 to -353 ppm. Clearly, an increase of coordination number around the tin centers shifts its NMR resonance to lower frequencies. This is consistent with the general trend observed for the Group 4A elements, *i.e.* an increase of coordination number increases the electron shielding and consequently causes an up-field shift of the isotropic CS value. The considerably smaller CSA spread of the distorted T_d tin in $(CHA)_4Sn_2S_6$, with respect to the pseudo-trigonal bipyramidal tin in the SnS-1 materials, indicates that the electron distribution around it is more symmetric.

TPA-SnS-3

The ^{119}Sn CP-MAS spectrum of TPA-SnS-3, collected at a spinning rate of 15 kHz with a contact time of 10 ms, is displayed in Fig. 4. Six distinct CSA patterns are resolved with isotropic CS values at -4.9, -20.2, -306.0, -320.6, -326.4 and -343.2 ppm. There are four crystallographically distinct tin sites in TPA-SnS-3, namely the three PTBP tin sites in one broken-cube cluster and the distorted T_d tin site that links the broken-cube clusters together, Fig. 5. Two of the PTBP tin sites have the same second coordination shell, *i.e.* one distorted T_d and two PTBP tin sites and are expected to have a similar CSA pattern. The third one has three PTBP tin sites in the second coordination shell, and is expected to have a distinct CSA pattern. In addition, the distorted T_d tin site is expected to give rise to another unique CSA lineshape. Therefore, in total three distinct CSA patterns are anticipated from a TPA-SnS-1 sample. The T_d tin is expected to be less shielded in comparison with the PTBP tin sites as discussed above and occurs at a higher resonance frequency. Therefore, the isotropic CS peaks at -4.9 and -20.2 ppm are assigned to the distorted T_d tin site. The occurrence of two bands in this range reveals the presence of two distinct T_d tin sites in the sample, although there is only one crystallographically distinct T_d tin site in the TPA-SnS-3 structure.[1] The four isotropic CS PTBP tin sites

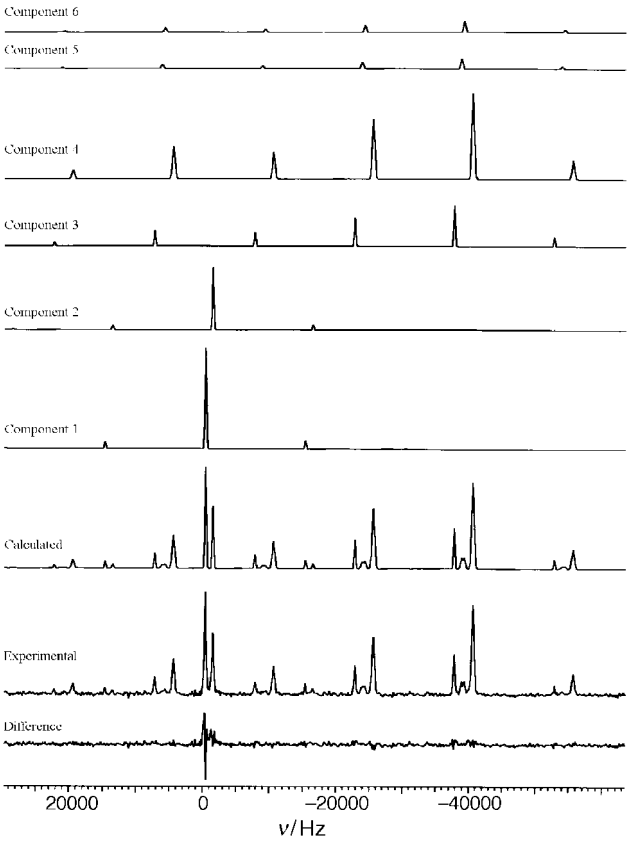

Fig. 4 The experimental and calculated ^{119}Sn CP-MAS NMR spectra of TPA-SnS-3, also showing the six calculated components

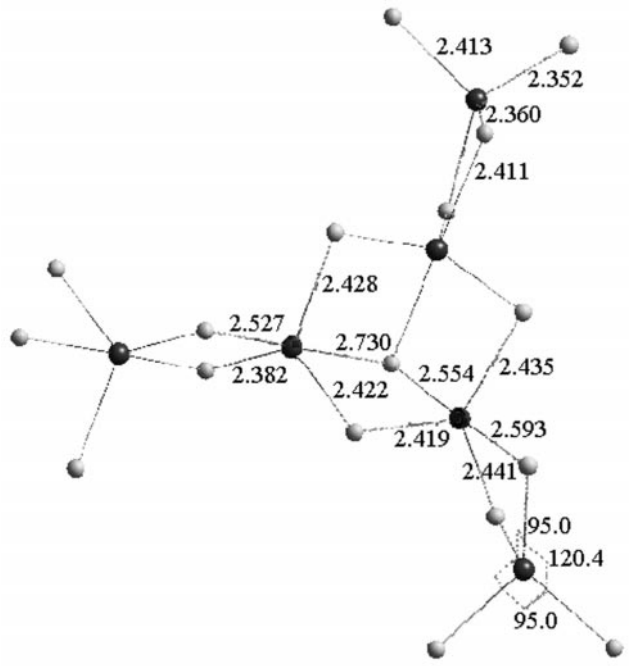

Fig. 5 An illustration of the local bonding geometry around the tin centers of TPA-SnS-3, important bond lengths and angles are displayed

are again twice as many as expected from the SCXRD structure data. This indicates that the sample contains an additional phase besides the TPA-SnS-3 phase. As discussed previously,[1] TPA-SnS-3 is pressure-sensitive and readily transforms to a second phase with a reduced lamellar spacing under moderate pressure, *e.g.* a modest grinding with a pestle and mortar. When packing the TPA-SnS-3 sample into the rotor for NMR

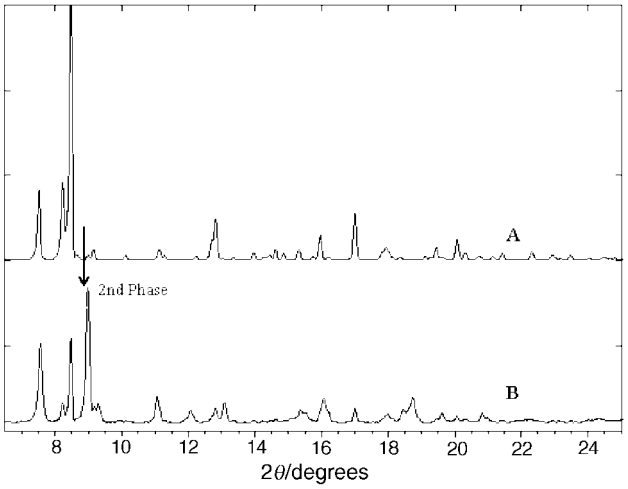

Fig. 6 PXRD patterns of TPA-SnS-3 (A) as-synthesized and (B) after ^{119}Sn CP-MAS NMR data collection

data collection, modest pressure was applied to the sample to assure sufficiently dense packing of the sample. This may have partially transformed the TPA-SnS-3 sample to the second phase. In addition, the fast spinning rate of the sample at 15 kHz during data collection provides a centrifugal force, imposing a certain degree of pressure on the sample and presumably further transforming it to the second phase. The PXRD pattern of the sample after data collection displayed in Fig. 6 clearly shows the presence of the second phase. Apparently, this new phase has resulted in more tin sites in the sample, and thus more CSA patterns. An inspection of the CSA lineshapes in Fig. 4 reveals that bands 1 and 2 feature rather similar lineshapes, and so do bands 3 and 4, and bands 5 and 6. Therefore, each pair most likely originates from tin sites that have a similar local electron density distribution and bonding character. As discussed earlier, three distinct CSA patterns are expected from the single crystal data of TPA-SnS-3,[1] thus the occurrence of three pairs of similar CSA patterns suggests that the Sn—S bonding and structure in the second phase resemble that of TPA-SnS-3, however with a small modification. This implies that this new phase is a modified TPA-SnS-3 phase. As revealed by the PXRD study, it has a different space group and unit cell dimensions compared to the original TPA-SnS-3 phase.

The similar CSA spread and lineshape of bands 3 and 4, Fig. 4, to those of the SnS-1 materials, Table 1, suggest that they originate from the PTBP tin sites that have three neighbouring SnS_5 units in the second coordination shell. Thus bands 5 and 6 are assigned to the PTBP tin site that has two SnS_5 and one SnS_4 unit in the second coordination shell. The electron distribution around this PTBP tin site is expected to be less symmetric, and to display a larger CSA width (about 140 kHz), in comparison to the other PTBP tin site (about 75 kHz).

The significantly smaller CSA spread of *ca.* 18 kHz observed for the distorted T_d tin site indicates that its local electron density distribution is more symmetric, with respect to that of the PTBP tin sites. In addition, it is also more symmetric than that of the distorted T_d tin site in $(CHA)_4Sn_2S_6$. For example, $(CHA)_4Sn_2S_6$ displays 12 spinning side bands at a spinning rate of 5 kHz and has a CSA spread of 54 kHz, while the T_d tin site in TPA-SnS-3 displays 7 spinning side bands at a spinning rate of 6.5 kHz with a CSA spread of 18 kHz. The T_d tin site in $(CHA)_4Sn_2S_6$ has two bridging and two terminal sulfurs with the corresponding Sn—S bond lengths of 2.45 and 2.33 Å, respectively. The negative charge is more likely centered on the terminal sulfurs. The four Sn—S bonds are significantly different in $(CHA)_4Sn_2S_6$, therefore a greater asymmetric

electron distribution is expected. Note that the isotropic CS value for the distorted T_d tin site in $Na_4Sn_3S_8$ is reported at -16.0 ppm with a large CSA width of 50 kHz at a spinning rate of about 2.5–4.5 kHz.[11] The structure of $Na_4Sn_3S_8$ is constituted of pseudo-trigonal bipyramidal SnS_5 and distorted tetrahedral SnS_4 building units. The tetrahedral tin also contains two bridging and two terminal sulfurs with the corresponding Sn—S bond lengths of 2.46 and 2.34 Å, respectively. It is interesting to note that the isotropic CS value observed for the distorted T_d tin in the framework of TPA-SnS-3 and $Na_4Sn_3S_8$ is considerably shifted upfield, by more than 70 ppm, in comparison with the dimeric $(CHA)_4Sn_2S_6$ and monomeric Na_4SnS_4. It seems that the distorted T_d tin(IV) site in tin sulfide frameworks has more electron shielding in comparison with the counterpart in molecular tin sulfide species.

^{119}Sn Mössbauer spectroscopy

The Mössbauer spectra of ATEA-SnS-1 and DABCOH-SnS-1 samples collected at room temperature are displayed in Fig. 7(A) amd (B). Both spectra are broad and may be fit to two peaks (see Experimental). In view of the pseudo-trigonal bipyramidal coordination environment around the tin sites in the SnS-1 structures, it is reasonable to ascribe the two components to a quadrupole splitting effect. Although there are three crystallographically distinct, pseudo-trigonal bipyramidal tin sites in the SnS-1 structure, they have similar local bonding character and presumably similar s-electron density at the nuclei and therefore should have similar isomer shift and quadrupole splitting values. The isomer shift (referenced to $CaSnO_3$) and quadrupole splitting values are summarized in Table 2. The small quadrupole splitting of *ca.* 0.5 mm s^{-1} suggests a relatively small electric field gradient around the pseudo-trigonal bipyramidal tin nuclei. This is consistent with the small asymmetry parameter of about 0.2 observed in the ^{119}Sn NMR spectra of these materials. The isomer shift is determined to be 1.11 and 1.12 mm s^{-1} in ATEA-SnS-1 and DABCOH-SnS-1, respectively, consistent with the presence of Sn^{IV}. This is in good agreement with the value of 1.19 mm s^{-1} reported for the pseudo-trigonal bipyramidal tin(IV) sites in $Na_4Sn_3S_8$.[12] The corresponding quadrupole splitting and linewidth were 0.54 and 0.84 mm s^{-1} in $Na_4Sn_3S_8$. The structure of $Na_4Sn_3S_8$ is based upon pseudo-trigonal bipyramidal SnS_5 and distorted tetrahedral SnS_4 building units. The isomer shift for the tetrahedral tin(IV) in $Na_4Sn_3S_8$ was reported to be 1.30 mm s^{-1} with a quadrupole splitting of 1.40 mm s^{-1}. Consistent with these values, the tetrahedral tin unit contains two bridging and two terminal sulfurs with Sn—S bond lengths of 2.46 and 2.34 Å, respectively. The considerable departure from a perfectly tetrahedral SnS_4 site and the large asymmetric electron distribution were believed to be responsible for its large quadrupole splitting of 1.40 mm s^{-1}. The linewidth is found to be 0.80 mm s^{-1} in ATEA-SnS-1 and 1.15 mm s^{-1} in DABCOH-SnS-1. The natural linewidth calculated from the lifetime of the excited state of the ^{119m}Sn nucleus is 0.642 mm s^{-1}, and the typical experimental value is 0.8 mm s^{-1} at best.[13] The crystallographically inequivalent tin sites in the SnS-1 materials presumably have introduced an additional line broadening. The greater linewidth observed for the DABCOH-SnS-1 sample implies that the three tin sites in the DABCOH-SnS-1 structure are less equivalent in terms of their local electron density distribution compared to ATEA-SnS-1. SC XRD data shows that the trigonal bipyramidal tin sites in ATEA-SnS-1 are less distorted than in DABCOH-SnS-1.[1] In addition, the phonons of the porous SnS-1 frameworks at room temperature are expected to cause certain line broadening.

As shown in Fig. 7(C), the Mössbauer spectrum of TPA-SnS-3 collected under experimental conditions similar to those of the ATEA-SnS-1 and DABCOH-SnS-1 samples, with 'triple' data collection time, displays considerably lower intensity and a higher signal-to-noise ratio. The microporous framework of TPA-SnS-3 contains 32-atom pores and is expected to be less rigid than those of the SnS-1 materials which contains 24-atom pores.[1,5] The rather flexible structure of TPA-SnS-3 implies that it will have a higher recoil energy or smaller

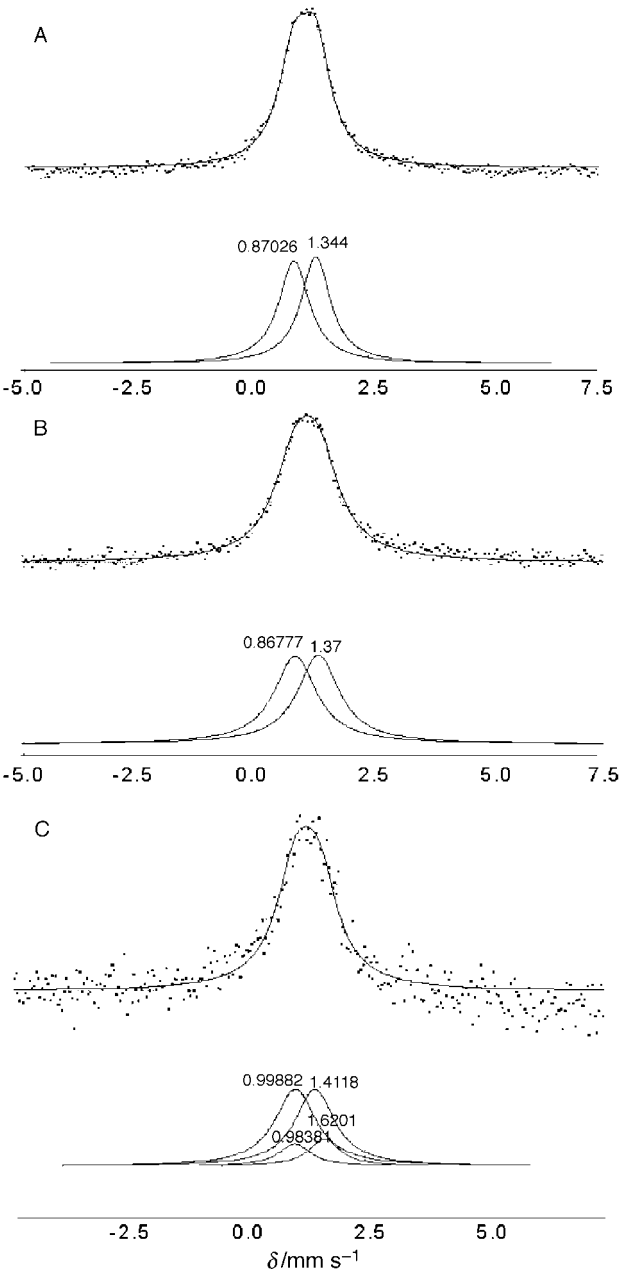

Fig. 7 The Mössbauer spectra of (A) ATEA-SnS-1, (B) DABCOH-Sn-1, and (C) TPA-SnS-3, collected at room temperature

Table 2 Summary of Mössbauer data for SnS-*n* materials

	C.N.	isomer shift[a]/ mm s^{-1}	quadrupole splitting[a]/ mm s^{-1}	linewidth[a]/ mm s^{-1}
ATEA-SnS-1	5	1.11	0.47	0.80
DABCOH-SnS-1	5	1.12	0.51	1.15
TPA-SnS-3	5	1.21	0.41	1.07
	4	1.30	0.64	0.85

[a]The χ^2 value obtained from the fitting of the SnS-1 samples is better than 0.985 whilst that for SnS-3 is around 0.87. Estimated error on deconvoluted isomer shifts, quadrupole splittings and linewidths is about ± 0.1 mm s^{-1}.

probability of recoil-free absorption than that of the SnS-1 materials. The lower recoil free fraction is believed to be mainly responsible for the low intensity and poor signal-to-noise ratio observed in Fig. 7(C). To improve the data quality, the sample has to be cooled to liquid nitrogen or helium temperature, which could not be performed during this work. Fitting of the room-temperature data was attempted. As discussed above, four crystallographically distinct tin sites are present in phase pure TPA-SnS-3 and ^{119}Sn CP-MAS NMR spectroscopy was able to resolve three sites. In the corresponding ^{119}Sn Mössbauer measurement, the four and five coordinated tin sites should have distinct isomer shift values. It is known in the literature that isomer shifts of tin centers generally decrease with an increase of coordination number.[13] For example, the isomer shift for the tetrahedral tin sites in $Na_4Sn_3S_8$ and Na_4SnS_4 were reported at 1.30 and 1.23 mm s^{-1}, respectively.[12] In contrast, the isomer shift for the octahedral tin site in Na_2SnS_3 and SnS_2 were observed at 1.02 and 0.8 mm s^{-1}, respectively. This is best interpreted in terms of a decrease of s-electron density at the tin nucleus with increase of coordination number, due to the screening effect of d electrons. When fitting the data, it is assumed that the three trigonal-bipyramidal tin sites have similar isomer shift and quadrupole splitting values to those of the SnS-1 materials and the tetrahedral tin has a higher isomer shift. As expected, greater intensity is associated with the SnS_5 relative to the SnS_4 sites, although it is difficult to compare the numbers with those expected crystallographically as their recoil-free fractions could be different. The numeric values obtained from the line-fitting are given in Table 2. However, the rather high χ^2 value of 0.87 and many fitting options that give similar χ^2 values indicate that a better data set is required for more reliable isomer shift and quadrupole splitting values. Note that the χ^2 value obtained from the fitting of the SnS-1 samples is better than 0.985.

Raman spectroscopy

The Raman spectra of the SnS-1 and SnS-3 materials are displayed in Fig. 8. The three to four diagnostic tin–sulfur stretching modes of the SnS-1 materials generally occur between 400 and 250 cm^{-1}; while the TPA-SnS-3 material feature two additional bands within this range. Factor group analysis shows that the tin sulfide framework of TMA-SnS-1 has 230 allowed unit cell vibrational modes, and at first glance it seems impossible to precisely assign the few observed bands. However, a local oscillator approach that considers the site symmetry of the constituent building blocks, namely pseudo-trigonal bipyramidal SnS_5 and distorted tetrahedral SnS_4, provides a fairly good interpretation of the observed vibrational bands. A trigonal-bipyramidal XY_5 with D_{3h} symmetry has six Raman active ($2A_1'$, 3E′, and E″) and five infrared active vibrations ($2A_2''$ and 3E′). Three stretching modes (ν_1, ν_2, ν_5) are Raman active and two (ν_3 and ν_5) are IR active. The relative frequencies for the four stretching modes are found to generally follow the order of $\nu_5 > \nu_3 > \nu_1 > \nu_2$, *i.e.* the equatorial bond stretching force constants are stronger than their axial counterparts.[14]

For the purpose of comparison, the three stretching modes ν_5, ν_1, ν_2 in the Raman spectrum of the trigonal-bipyramidal $[SnCl_5]^-$ anion in $[Bu^tPCl_3][SnCl_5]$ occur at 353 (medium), 338 (very strong) and 269 (weak) cm^{-1}.[15] Interestingly, the Raman spectra of the SnS-1 materials displays a very similar vibrational pattern to that of the $[SnCl_5]^-$ anion. For example, ATEA-SnS-1 and TEA-SnS-1 show three dominant bands at 367 (medium), 339 (very strong), 286 (weak) cm^{-1} and 362 (medium), 338 (very strong), 277 (weak) cm^{-1}, respectively, see Fig. 8(A) for ATEA-SnS-1. Cs-SnS-1 also exhibits three Sn—S stretching bands at 360 (medium), 336 (very strong), 284 (weak) cm^{-1} in its Ramam spectrum.[16] In DABCOH-SnS-1, Fig. 8(A), an additional band at 322 cm^{-1} is observed corresponding to a weak shoulder in ATEA-SnS-1. In a pseudo-trigonal bipyramidal AB_5 molecule, the distortion from perfect D_{3h} symmetry may split the ν_5 mode into two bands, and/or make the ν_3 mode Raman active. Both cases would result in more Raman stretching modes. Also deviations from the local oscillator approximation (*e.g.*, correlation coupling) could produce some extra band splitting. Interestingly, the Raman spectrum of $K_2Sn_2S_5$ displays four strong stretching modes in the Sn—S vibrational range, at 367, 346, 334 and 270 cm^{-1}.[17] The 3D open framework of $K_2Sn_2S_5$ is entirely built up of distorted trigonal-bipyramidal SnS_5 building units, with the K^+ cations residing inside the channels.

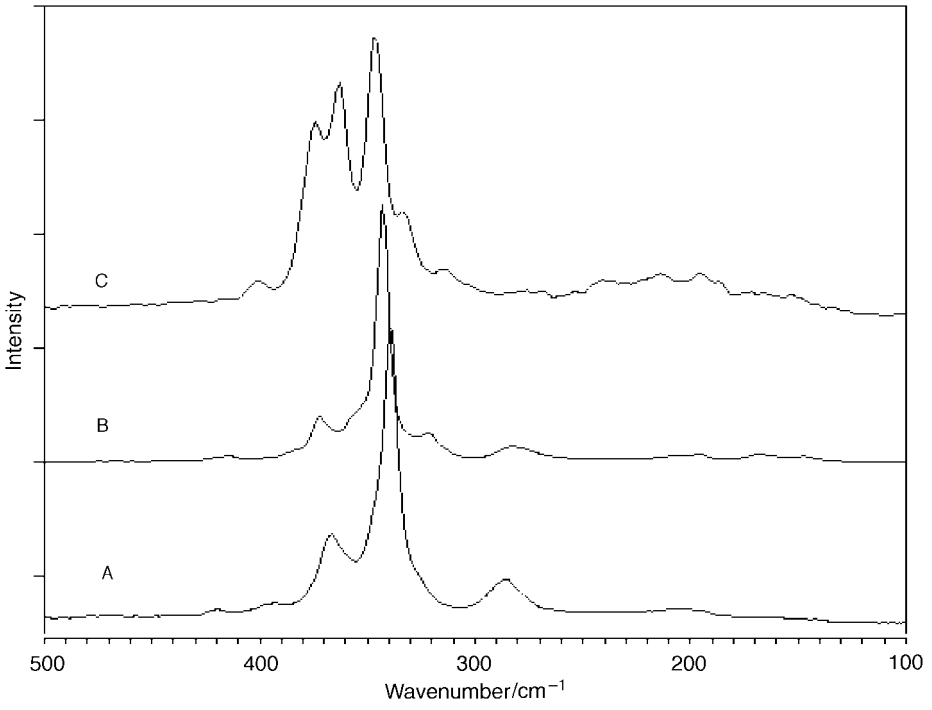

Fig. 8 FT-Raman spectra of (A) ATEA-SnS-1, (B) DABCOH-SnS-1 and (C) TPA-SnS-3

The framework of TPA-SnS-3 also contains a distorted tetrahedral tin site besides the PTBP ones. For a perfect tetrahedral AB_4 molecule, there are four Raman and two infrared active vibrational modes. The two stretching modes v_1 and v_3 are both Raman active, and generally $v_3 > v_1$. Therefore, the two additional Raman modes at 401 and 374 cm^{-1} in Fig. 8(C) are best assigned to the distorted SnS_4 building unit. The higher stretching frequencies associated with the SnS_4 unit are consistent with the shorter (by *ca.* 0.15–0.2 Å) and stronger Sn—S bonds relative to those in the SnS_5 unit. A comparison of the Raman stretching modes in various tin compounds is listed in Table 3.

Optical spectroscopy

The electronic and optical properties of bulk SnS_2 have been studied quite extensively.[18] Various authors have calculated its electronic structure employing the 'pseudopotential method' and 'tight-binding method'.[19] Robertson has reported that SnS_2 has an indirect band gap of 2.48 eV ($G_2^- \rightarrow L_1^+$) and a direct band gap of 2.66 eV ($G_2^- \rightarrow G_1^+$).[20] The valence band is about 8 eV in width, the top of which is primarily constituted by the 3p orbitals of the S^{-II}. The bottom of the conduction band mainly contains the 5p orbitals of Sn^{IV}. The main optical transition is assigned to S^{-II}, 3p$\rightarrow Sn^{IV}$, 5p indirect transitions. Although the SnS-1 and SnS-3 materials feature a 2D structure as in bulk SnS_2, their tin sulfide sheets are perforated by a regular array of hexagonal or elliptical pores. Crystalline porous semiconductors have been viewed as quantum antidot lattices, the geometric complement of a quantum dot lattice.[9] Blue shifted bad gaps, excitonic absorptions and strong luminescence, as observed for quantum dots, are also expected from porous semiconductor 'antidots'. Kanatzidis and coworkers have investigated the electronic and optical properties of a series of low dimensional and open-framework cadmium chalcogenides, with respect to bulk CdS.[21] It was discovered that these materials mimic physically small clusters. They have attributed the blue-shifted band gaps of open-framework cadmium chalcogenides with respect to bulk phase to their lower framework connectivity or lower coordination number of component atoms. The microporous SnS-*n* materials are also expected to display some unique electronic and optical properties with respect to dense packed SnS_2.

Single crystal optical absorption

Single crystals of DABCOH-SnS-1, ATEA-SnS-1 and dimeric $(CHA)_4Sn_2S_6$ (CHA = cyclohexylammonium) were used for variable temperature UV–VIS absorption measurements. Fig. 9 displays the results for DABCOH-SnS-1 and $(CHA)_4Sn_2S_6$, the corresponding crystal thicknesses are 520 and 280 μm, respectively. The optical quality of sample crystals was first examined under a microscope between crossed polarizers, and extinction directions were determined. It was found that the polarization direction had no significant effect on the absorption band intensities and positions. The spectra presented in Fig. 9 were collected using unpolarized light and not for any specific crystal orientation. They all show a steep rise of the absorption edge that shifts to higher energy at lower temperatures. The steep increase of the intensity of the absorption band is rapidly cut off by the stray light limiter. The minimum molar absorptivity can be estimated to be about 2×10^4 M^{-1} cm^{-1} for all the samples at the absorption edge, which is very close to that determined for dimeric $(CHA)_4Sn_2S_6$ in aqueous solution.[1] The corresponding absorption in $(CHA)_4Sn_2S_6$ was assigned to a S^{-II} to Sn^{IV} LMCT type electronic transition. The high intensity of the absorption bands shown in Fig. 9 suggests an allowed electronic transition in the dimer and SnS-1 materials. This would imply that the observed negative temperature dependence of the band gap mainly originates from lattice contraction and greater overlap of tin and sulfur orbitals at low temperatures, resulting in a larger band gap.

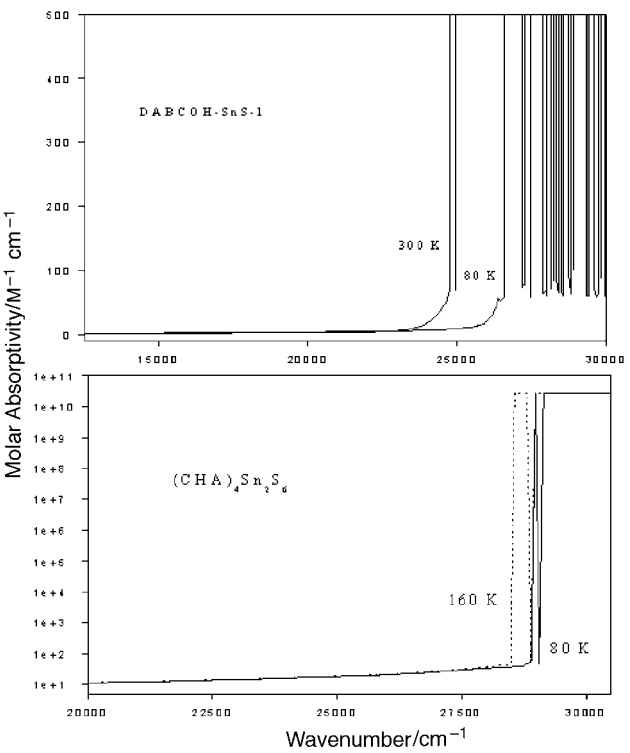

Fig. 9 Single crystal UV–VIS absorption spectra of (top) DABCOH-SnS-1 and (bottom) $(CHA)_4Sn_2S_6$

The energy of the absorption onset at room temperature can be estimated to be 3.53 eV for dimeric $(CHA)_4Sn_2S_6$ and 3.07 eV for the SnS-1 materials. The band gap of SnS_2 is calculated to be 2.48 eV, and the experimental value is 2.31 eV,[22] while the band gap of the channel-structured $K_2Sn_2S_5$ framework is reported to be 2.36 eV.[17] The blue-shifted band gap of the microporous layered SnS-*n* materials with respect to bulk SnS_2 may be explained in terms of the reduced connectivity of the component tin and sulfur atoms. In bulk SnS_2, all of the tin atoms are 6-coordinated and all of the sulfurs are 3-coordinated; while in SnS-1, tin atoms are 5- and sulfurs are 3- and 2-coordinated. The lower coordination numbers of both tin and sulfur in the SnS-1 structures may have reduced the overlap of the constituent orbitals and narrowed the bands, and consequently resulted in an enlarged band gap. The 3D channel structure of $K_2Sn_2S_5$ contains 5- and 2-coordinated tin and sulfur, respectively. The higher dimensionality of $K_2Sn_2S_5$, however, gives a larger framework connectivity and orbital overlap, and thus a broader band width, with respect to the 2D SnS-1 structure. The band gap of $K_2Sn_2S_5$ is found to be very close to that of bulk SnS_2 and

Table 3 A comparison of Sn–L Raman stretching frequencies for various tin(IV) solid state materials

	local symmetry of the tin center	Sn–L stretching frequency/cm^{-1}
$[BuPCl_3][SnCl_5]$	PTBP	353 (m), 338 (vs), 269 (w)
ATEA-SnS-1	PTBP	367 (m), 339 (vs), 286 (w)
TEA-SnS-1	PTBP	362 (m), 338 (vs), 277 (w)
Cs-SnS-1	PTBP	360 (m), 336 (vs), 284 (w)
DABCOH-SnS-1	PTBP	372 (m), 343 (vs), 322 (w), 282 (w)
$K_2Sn_2S_5$	PTBP	367 (vs), 346 (s), 334 (w), 270 (m)
TPA-SnS-3	PTBP, T_d	363 (s), 346 (vs), 333 (m), 314 (w), 401 (w), 374 (s)

significantly smaller than the 2D microporous SnS-*n* materials. Dimeric $(CHA)_4Sn_2S_6$ is characterized by HOMO and LUMO orbitals with the largest energy separation, therefore its optical edge appears at the highest energy in comparison with 2D and 3D tin sulfides.

Luminescence and excitation

The photoluminescence spectra of DABCOH-SnS-1 as a function of temperature are displayed in Fig. 10. The lowest energy band at about 15 100 cm^{-1} appears only at temperatures lower than 40 K. All the luminescence bands exhibit higher intensities at lower temperatures implying that non-radiative relaxation pathways are reduced. The onset of the luminescence band at about 23 000 cm^{-1} is close to the onset of the absorption edge shown in Fig. 9. This suggests that the Stokes shifted luminescence originates from band gap emission. An inspection of the luminescence spectra reveals that the broad band at 23 000 cm^{-1} actually contains many components. The deconvoluted peak positions are 15 100, 19 900, 21 300 and 22 800 cm^{-1}. This is further confirmed by an excitation study of this material as shown in Fig. 11. The excitation wavelengths used, 470 nm (21 275 cm^{-1}) and 500 nm (20 000 cm^{-1}), were chosen to be close to two of the luminescence bands occurring at 19 900 cm^{-1} and 21 300 cm^{-1}, respectively. Two distinct excitation bands are obtained, showing that the Stokes shifted luminescence and the absorption edge contain multiple states. The onset of both excitation spectra occurs at almost the same energy, 26 200 cm^{-1} for detection at 500 nm and 26 700 cm^{-1} for 470 nm. This is close to the high-energy onset of the luminescence spectra, Fig. 10. This indicates that the primary luminescence originates from states that are close to the conduction band edge. It appears that the conduction band width of the SnS-1 materials is quite narrow. This is consistent with the low dimensionality (2D) and microporous structural feature, and the observed blue-shifted band edge of these materials with respect to 3D open-framework tin sulfide and 2D dense packed SnS_2. These are indications that quantum size effects may contribute to the electronic and optical properties of SnS-1 materials. Note that the luminescence life time of the band gap emission has been measured on a TMA-SnS-1 sample at 20 K with a detection frequency of 470 nm. The life time is estimated to be 100 ns, implying a direct band electronic description for the SnS-1 materials.[2]

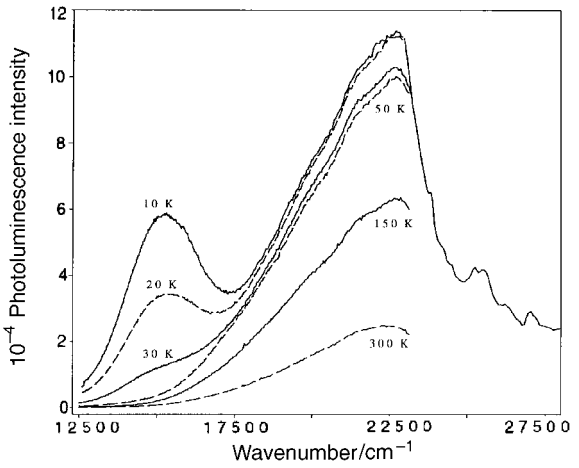

Fig. 10 Temperature dependent photoluminescence spectra of DABCOH-SnS-1

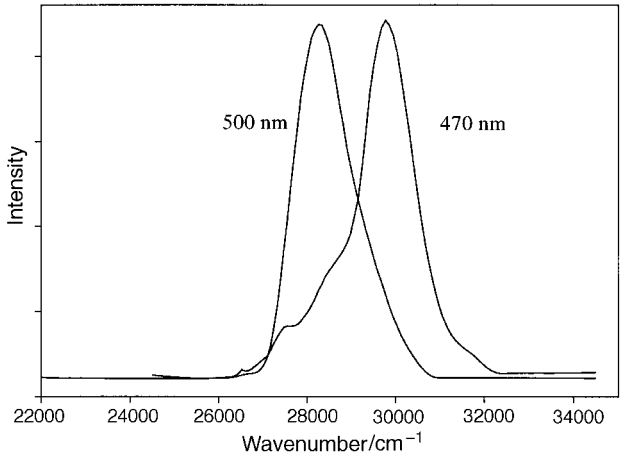

Fig. 11 Excitatin spectra of DABCOH-SnS-1 detected at 470 and 500 nm at 10 K

Conclusions

The ^{119}Sn NMR and ^{119}Sn Mössbauer spectroscopy results show that the three crystallographically distinct tin sites in the SnS-1 materials have similar local bonding and electron density distributions that cannot be resolved by either ^{119}Sn NMR or ^{119}Sn Mössbauer spectroscopies. The chemical shift for the pseudo-trigonal bipyramidal tin site in the SnS-1 materials occurs around -340 to -354 ppm, relative to Me_4Sn, with a large CSA width of almost 80 kHz. The corresponding isomer shift occurs at around 1.1 mm s^{-1}, relative to $CaSnO_3$. The rather small asymmetry parameter η (*ca.* 0.2) of the NMR CSA tensors and the small Mössbauer quadrupole splitting of about 0.5 mm s^{-1} suggest the local bonding and electron distribution around the pseudo-trigonal bipyramidal tin sites is quite symmetric. The pseudo-trigonal bipyramidal tin site in TPA-SnS-3, that has two pseudo-trigonal bipyramidal and one pseudo-tetrahedral tin sites in the second coordination shell, has a larger CSA width (*ca.* 140 kHz) compared with the counterpart that has three pseudo-trigonal bipyramidal tin sites in the second coordination shell (*ca.* 76 kHz). The four coordinated pseudo-tetrahedral tin sites in TPA-SnS-3 has unique chemical shift and isomer shift values around 0 to -22 ppm and 1.30 mm s^{-1}, respectively. The NMR chemical shift moves downfield (more shielded) with an increase of coordination number while the Mössbauer isomer shift decreases. The framework of TPA-SnS-3 appears to be quite flexible compared to the SnS-1 structure (low recoil-free fraction), therefore to obtain high quality Mössbauer data, the sample will have to be cooled to cryogenic temperatures. Note that the dimeric $(CHA)_4Sn_2S_6$ does not give any Mössbauer signal at room temperature presumably because the recoil-free fraction associated with this molecular species is low. It should be mentioned that Mössbauer spectroscopy has proven to be an excellent probe for detection of the dense packed impurities in the SnS-*n* samples. The most common ones are SnO_2, SnS_2 and Sn. Their rigid structures confer a high recoil-free absorption, and consequently they display much higher intensity than the more flexible microporous layered SnS-*n* materials. A local oscillator approximation, involving the symmetry allowed stretching modes associated with the pseudo-trigonal bipyramidal and pseudo-tetrahedral tin sulfide building-blocks that make up the microporous layered tin sulfide framework, appears to provide a satisfactory description of the Raman vibrational properties of the SnS-*n* materials. The single crystal absorption, luminescence and excitation spectroscopic properties of DABCOH-SnS-1 suggest that it has a direct band gap of 3.07 eV. In comparison, bulk SnS_2 has an indirect band gap of 2.48 eV.[22] A 3D open-framework $K_2Sn_2S_5$ has a band gap of 2.36 eV.[17] Luminescence and excitation spectra of DABCOH-SnS-1 suggest that the conduction band width of DABCOH-SnS-1 is fairly narrow, which is consistent with its observed larger band gap compared to SnS_2 and $K_2Sn_2S_5$. In comparison with the 2D close-packed structure of bulk SnS_2, the coordi-

nation number of the constituent tin and sulfur atoms in DABCOH-SnS-1 is smaller, and in comparison with the 3-D open structure of $K_2Sn_2S_5$, DABCOH-SnS-1 has a reduced dimensionality. These structural differences result in reduced tin–sulfur orbital overlaps in DABCOH-SnS-1, consequently leading to narrower bands and a larger band gap.

Experimental

Materials

Synthetic and structural properties of TEA-SnS-1, ATEA-SnS-1, DABCOH-SnS-1 and $(CHA)_4Sn_2S_6$ have recently been described.[1–4]

Powder X-ray diffraction (PXRD)

PXRD patterns were obtained on a Siemens D5000 diffractometer employing a high power Cu-Kα X-ray source and a Kevex solid state detector. For *in situ* VT-PXRD measurements in nitrogen, a heating rate of 10 °C min^{-1} was used and temperature ramping was stopped during data collection.

NMR Spectroscopy

^{119}Sn MAS and ^{1}H/^{119}Sn CP-MAS NMR data were recorded on a Bruker DSX 200 spectrometer with a typical recycle delay of 10–20 s, a CP contact time of 2–20 ms and spinning rate of 5–15 kHz. Data were fitted by the Herzfeld and Berger method[10] and chemical shifts were referenced to $SnMe_4$.

Mössbauer spectroscopy (MS)

MS spectra were recorded at room temperature on a Ranger Scientific MS-200 constant acceleration spectrometer. The γ-ray source used was 5 mCi ^{119m}Sn in a $CaSnO_3$ matrix at room temperature. Isomer shift (IS) values were referenced to $CaSnO_3$ (0.0 mm s^{-1}). The spectra were fitted to a convolution of Lorentzian functions by a least-squares method, using in-house software. The χ^2 value obtained from the fitting of the SnS-1 samples is better than 0.985 whilst for SnS-3 it is about 0.87. The estimated error on deconvoluted isomer shifts, quadrupole splittings and linewidths is about $\pm$0.1 mm s^{-1}.

Fourier transform Raman (FT-Raman) spectroscopy

The FT-Raman spectra were recorded on a Bomem MB-157 Fourier transform spectrometer equipped with an InGaAs near-IR detector and a diode pumped Nd:YLF laser emitting at 1064 nm. Notch filters covering a range of 150–3750 cm^{-1} were employed to block the Rayleigh scattering. The spectrometer was configured in a 180° back scattering mode.

Optical spectroscopy

Single crystal optical absorption data were recorded on a Varian Cary 5 double beam spectrophotometer. Samples were mounted in a helium gas-flow cryostat (Oxford Instruments CF 1204). A 150 W Xe arc lamp filtered through a $CuSO_4$ solution and a Schott UG 1 filter was used as excitation source for luminescence spectra. For the energy region higher than 23 000 cm^{-1}, the source of light from the Xe lamp was filtered through a Spex 500M 0.5 m monochromator. The luminescence data were recorded using a Spex 1800-II 0.75 m monochromator, and a Schott KV 418 long-pass filter was placed in front of the entrance slit of the monochromator. The detection system consisted of a Hamamatsu R4632 photomultiplier connected to a Stanford Research SR 400 photon counter.

G.A.O. is deeply indebted to the Killam Foundation for an Issac Walton Killam Research Fellowship for the period 1995–97. Generous financial support of this work by the Natural Sciences and Engineering Research Council of Canada (NSERC), Universal Oil Products (UOP) and the Canadian Space Agency (CSA) is deeply appreciated. T.J. is grateful for graduate scholarships from the University of Toronto. The assistance of Dr. Patricia Aroca with solid state NMR spectroscopy, Dr. Ömer Dag with FT-Raman and Mössbauer spectroscopies, Dr. Srebri Petrov with PXRD, and Dr. Christian Reber at the University of Montreal with single optical measurements of SnS-*n* materials, is deeply appreciated.

References

1 T. Jiang, R. L. Bedard, R. Broach, A. Lough and G. A. Ozin, *J. Mater. Chem.*, 1998, **8**, 721; G. A. Ozin, T. Jiang and A. Lough, A. *Adv. Mater.*, 1998, **10**, 42; T. Jiang, R. L. Bedard, A. J. Lough, G. A. Ozin, S. Petrov and D. Young, *Chem. Mater.*, 1995, **7**, 245.
2 G. A. Ozin, R. L. Bedard, C. L. Bowes, N, Coombs, Ö. Dag, T. Jiang, A. Lough, S. Petrov, I. Sokolov, A. Verma, G. Vovk and D. Young, *Adv. Mater.*, 1997, **9**, 1133; G. A. Ozin, R. L. Bedard, C. L. Bowes, N. Coombs, Ö. Dag, T. Jiang, A. Lough, S. Petrov, I. Sokolov, A. Verma, G. Vovk and D. Young, *Nature*, 1997, **388**, 857.
3 G. A. Ozin, P. Enzel, R. L. Bedard and G. S. Henderson, *Adv. Mater.*, 1995, **7**, 64.
4 T. Jiang, G. A. Ozin, R. L. Bedard and A. Lough, *J. Mater. Chem.*, 1998, **8**, 733; T. Jiang, G. A. Ozin and D. Young, *Adv. Mater.*, 1994, **6**, 860.
5 H. Ahari, R. L. Bedard, C. L. Bowes, T. Jiang, A. J. Lough, G. A. Ozin, S. Petrov and D. Young, *Adv. Mater.*, 1995, **7**, 375.
6 T, Jiang, R. L. Bedard and G. A. Ozin, *Adv. Mater.*, 1995, **7**, 166.
7 H. Ahari, R. L. Bedard, C. L. Bowes, T. Jiang, G. A. Ozin and D. Young, *US Patent*, 5,594,263, **1997**; G. A. Ozin, *Supramol. Chem.*, 1995, **6**, 125; T. Jiang, G. A. Ozin, A. Verma and R. Bedard, *J. Mater. Chem.*, following paper.
8 C. L. Bowes, S. Petrov, G. Vovk, D. Young, G. A. Ozin and R. L. Bedard, *J. Mater. Chem.*, 1998, **8**, 711; G. A. Ozin and C. L. Bowes, *Adv. Mater.*, 1996, **8**, 13.
9 G. A. Ozin, *Adv. Mater.*, 1992, **4**, 612; M. A. Reed, *Sci. Am.*, 1993, 118.
10 J. Herzfeld and A. E. Berger, *J. Chem. Phys.*, 1980, **73**, 6021.
11 C. Mundus, G. Taillades, A. Pradel and M. Ribes, *Solid State Nucl. Magn. Reson.*, 1996, **7**, 141.
12 R. Greatrex, N. N. Greenwood and M. Ribes, *J. Chem. Soc., Dalton Trans.*, 1976, 500.
13 A. Vértes, L. Korecz and K. Burger, *Mössbauer Spectroscopy*, Akadémiai Kiadó, Budapest, 1979; *Mössbauer Spectroscopy Applied to Inorganic Chemistry*, ed. G. J. Long, Plenum Press, New York, 1984.
14 *Infrared and Raman Spectra of Inorganic and Coordination Compounds*, ed. K. Nakamoto, John Wiley & Sons, Inc., New York, 1986, 4th edn.
15 J. I. Bullock, N. J. Taylor and F. W. Parrett, *J. Chem. Soc., Dalton Trans*, 1972, 1844.
16 G. A. Marking and M. G. Kanatzidis, *Chem. Mater.*, 1995, **7**, 1915.
17 J. Liao, C. Varotsis and M. G. Kanatzidis, *Inorg. Chem.*, 1993, **32**, 2453.
18 E. Lifshitz, Z. Chen and L. Bykov, *J. Phys. Chem.*, 1993, **97**, 238, and references therein.
19 (*a*) C. Y. Fong and M. L. Cohen, *Phys. Rev. B*, 1972, **5**, 3095; (*b*) R. B. Murray and R. H. Williams, *J. Phys. C: Solid State Phys.*, 1973, **6**, 3643; (*c*) J. Bordas, J. Robertson and A. Jakobsson, *J. Phys. C: Solid State Phys.*, 1978, **11**, 2607.
20 J. Robertson, *J. Phys. C: Solid State Phys.*, 1979, **12**, 4753.
21 E. A. Axtell III, J.-H. Liao, Z. Pikramenou and M. G. Kanatzidis, *Chem. Eur. J.*, 1996, **2**, 656; E. A. Axtell III, J.-H. Liao, Z. Pikramenou, Y. Park and M. G. Kanatzidis, *J. Am. Chem. Soc.*, 1993, **115**, 12191.
22 M. J. Powell and A. J. Grant, *Nuovo Cimento B*, 1977, **38**, 486.

Paper 8/01602J; *Received* 25*th February*, 1998